Chemical and Process Engineering: New Frontiers, 2023, 44(1), e3
DOI: 10.24425/cpe.2023.142292

Influence of changes in liquid circulation on the mixing power when emptying the tank with a rotating 6FBT impeller

Jacek Stelmach[1]*, Czesław Kuncewicz[1], Tomáš Jirout[2], František Rieger[2]

[1] Lodz University of Technology, Faculty of Process and Environmental Engineering, Wólczańska 213, 93-005 Łódź, Poland
[2] Czech Technical University in Prague, Faculty of Mechanical Engineering, Technická 4, 166 07 Praha 6, Czech Republic

*** Corresponding author:**
e-mail:
jacek.stelmach@p.lodz.pl

Article info:
Received: 01 December 2022
Revised: 09 January 2023
Accepted: 29 March 2023

Abstract
This study presents the results of tests on the mixing power and distribution of three velocity components in the mixing tank for an FBT impeller during tank emptying with an operating impeller. A laser PIV system was used to determine speed distributions. It was found that for the relative liquid height in the tank $H^* = H/H_0 \approx 0.65$ and $H^* \approx 0.45$, the liquid circulation in the impeller zone changed from radial to axial and vice versa. These changes were accompanied by changes in the mixing power which even reached 40%.
In the theoretical part, a method of calculating the mixing power using the classical model of the central vortex and distribution of the tangential speed in the impeller zone was proposed. Although the method turned out to be inaccurate, it was useful for determining the relative power.

Keywords
FBT impeller; mixing; power consumption; tank emptying

1. INTRODUCTION

In turbulent regime of motion, for mixing two-phase liquid-liquid, liquid-solid, liquid-gas or three-phase systems, we usually use small-diameter impellers, i.e. Rushton turbine, flat-blade turbine impellers (6FBT impellers), pitched-blade turbine impellers (6PBT) or propeller impellers (Ghotli et al. 2013, Nagata, 1975, Paul et al., 2004; Zhao et al., 2011). The first two types of impellers are called radial impellers. They reject a stream of liquid from the mixing zone mainly in the horizontal direction, and this type of impellers is mainly used for mixing liquid-liquid or liquid-gas systems. The other two types are axial impellers, where the main liquid stream flowing from the impeller zone is the axial stream and we use them for mixing liquid-solid suspensions. Regardless of the type of agitator, all of them are often used in biochemical reactors (Aiba et al., 1973; Cașcaval et al., 2011; Campesi et al., 2009; Delvigne et al., 2006; Galaction et al., 2004; Mohammed et al., 2008). If, in the technological process carried out in industrial conditions, it is necessary to remove the contents of the mixer while the stirrer is rotating, then as the free surface of the liquid approaches the area of the stirrer, large changes in the power requirement for the stirrer drive occur. This phenomenon has been observed relatively recently (Mazoch et al., 2016) and despite its importance, it has not been sufficiently described so far.

During our previous research on the increase of mixing power when emptying the tank with an operating axial impeller (6PBT impellers), (Rieger et al., 2021; Stelmach et al., 2020) a similar series of tests was also performed for an impeller with a blade inclination angle of $\alpha = 90^\circ$ (6FBT), which was a classic radial impeller. The power curves obtained for this impeller had a completely different course than those of other pitched blade impellers. For operating 6PBT impellers, when the value of Froude number $\mathrm{Fr} = N^2 \cdot D/g$ did not exceed $\mathrm{Fr} = 0.3$ and when the dimensionless height of the liquid above the impeller was very small and amounted to $(H - C)/T \approx 0.1$, an abrupt increase of mixing power (even up to 100%) was observed (Stelmach et al., 2020). In the case of the 6FBT impeller with vertical blades, the course of the changes was substantially different. The changes started already at $(H - C)/T \approx 0.3$ and, unlike the PBT impellers, there was first a relatively fast reduction in mixing power, and then it returned to the initial value: only when the impeller emerged from the liquid did the mixing power gradually decrease to zero for obvious reasons. The differences in power demand of 6PBT impellers resulted from the changes in liquid circulation in the mixing tank and changes in the hydrodynamics of the liquid flow near the tips of the impeller blades. A detailed description of the mechanism of this phenomenon can be also found elsewhere (Stelmach et al., 2020; Stelmach et al., 2021a; Stelmach et al., 2021b).

The impeller blades transmit energy to the liquid and dissipation occurs outside the impeller area. Therefore, changes in hydrodynamics in the impeller area are important in explaining changes in mixing power when emptying the tank. The theory of the central vortex (Nagata, 1975) indicates that in the absence of baffles the liquid inside the impeller, up to the radius R_c ($R_c < R_{\mathrm{imp}}$), rotates at a constant angular velocity ω without a velocity gradient in the circumferential

direction, where ω, rad/s is the rotational frequency of the impeller.

$$R \leq R_c U_t = R \cdot \omega \tag{1}$$

For a radius greater than R_c the tangential velocity of the liquid decreases hyperbolically with the radius according to this relationship.

$$R \geq R_c U_t = \frac{\omega \cdot R_c^2}{R} \tag{2}$$

The value of radius R_c, for which liquid velocity reaches the maximum value can be calculated from two equations. The first is the equation given in Nagata's monograph (Nagata, 1975):

$$R_{c1} = R_{\text{imp}} \cdot \frac{\text{Re}}{1000 + 1.6 \cdot \text{Re}} \tag{3}$$

where: R_{imp} – impeller radius ($R_{\text{imp}} = D/2$), m, $\text{Re} = N \cdot D^2 \cdot \rho/\eta$ – Reynolds number for the mixing process. The second equation is the experimentally obtained relationship (Stręk, 1971):

$$R_{c2} = R_T \cdot \exp\left[\frac{1}{2} + \frac{n_1^2}{2n_1 + 0.544\left(\frac{R_{\text{imp}}}{R_T}\right)^{1.46}} - \frac{R_T^2}{R_y^2}\right] \tag{4}$$

in which: $R_T = T/2$ – radius of the mixing tank, m, n_1 – the so-called number of inflows (sources) and outflows ($n_1 = 4$ for the impeller standard position), R_y – vortex radius at the level of the static liquid height H_0 and it is calculated from Equation (5):

$$R_y = R_T \cdot \left[0.508 + 0.215 \cdot \left(\frac{R_{\text{imp}}}{R_T}\right)\right] \tag{5}$$

According to the literature (Stręk, 1971), the R_{c2} values calculated from Equation (4) may be overestimated, especially for not very high values of the Reynolds number.

The profile of tangential velocity in the sensitive area of the mixing tank, which is the impeller zone, is also described by the empirical relationship (6) (Stręk, 1971):

$$U_t = \begin{cases} k \cdot \dfrac{R}{2} \cdot \left(2 - \dfrac{R^2}{R_{\text{imp}}^2}\right) & \text{for } 0 < R < R_{\text{imp}} \\ k \cdot \dfrac{R_{\text{imp}}^2}{2 \cdot R} & \text{for } R > R_{\text{imp}} \end{cases} \tag{6}$$

in which the coefficient $k = (\mathrm{d}U_t/\mathrm{d}R)_R = 0$ is determined experimentally.

Relationships (1), (2), and (6) are presented graphically in Figure 1. The dark gray area in the figure is the area where there are velocity differences, and it is responsible for energy transfer by the blades to the liquid. The case for which the value Re_{c1} calculated from Equation (3) for the classic model of the central vortex is marked in light grey and both gray

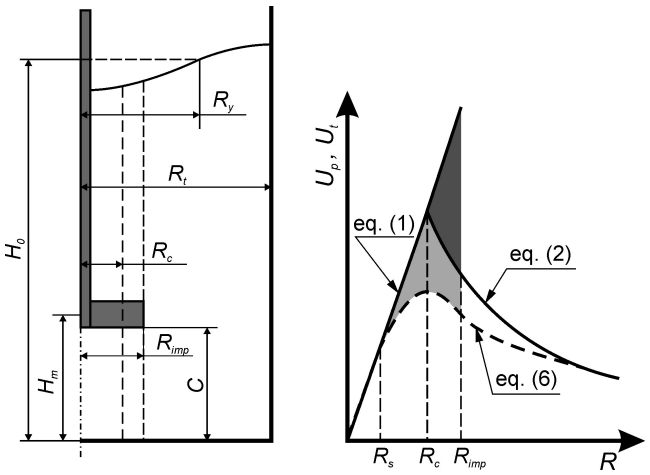

Figure 1. Diagram of the central vortex formation.

colors indicate the case where the value of U_t is determined by Equation (6). As is shown in Figure 1, on the radius of the impeller $R_s < R < R_{\text{imp}}$, the difference of the tangential velocities ΔU of the blade and the liquid is different for different values of R. However, from Equation (7) it is possible to calculate the integral mean of this difference:

$$\overline{\Delta U} = \frac{1}{R_{\text{imp}} - R_s} \int_{R_s}^{R_{\text{imp}}} [U_p(R) - U_t(R)]\,\mathrm{d}R \tag{7}$$

where: R_s – radius for which the liquid velocity becomes lower than the velocity of the impeller blade, m, $U_p(R)$ – tangential velocity of the impeller blade at a distance R from the axis of rotation, m/s, $U_t(R)$ – velocity of the liquid tangential component at a distance R from the axis of rotation of the impeller, m/s. The integral value (7) can be calculated numerically if the profile of the tangential velocity of the liquid between the impeller blades is known.

On a moving blade drag force acts (Paul et al., 2004) determined by the basic relationship (8)

$$F = C_d \cdot A \cdot \frac{\Delta U^2}{2} \cdot \rho \tag{8}$$

in which: C_d – drag coefficient of the impeller blade, A – blade surface area perpendicular to the velocity direction, m^2, ΔU – blade velocity in relation to the motionless fluid (relative velocity), m/s, ρ – liquid density, kg/m^3. For turbulent flow, the drag coefficient C_d has a constant value (Ortiz et al., 2012; Ortiz et al., 2015) and for perpendicular flow around the plate the value $C_d \approx 1.2$ is often used (Hargreaves et al., 2014; Ortiz et al., 2015). Therefore, from the model point of view, for a fixed rotational frequency of the impeller N, changes of the mixing power should be related primarily to the changes of the blade and liquid velocity ΔU.

The relationship between the drag force and the mixing power is described by the relationship:

$$P = 2 \cdot \pi \cdot N \cdot M \cdot z = 2 \cdot \pi \cdot N \cdot F \cdot R_F \cdot z \tag{9}$$

in which: M – torque $M = F \cdot R_F$, Nm, R_F – distance from the axis to the F force application point, m, z – number of impeller blades. If we assume that due to the narrow range from R_{imp} to R_s, the value of R_F is constant, and using Equation (7) after simple algebraic transformations we get:

$$Eu = \frac{P}{N^3 \cdot D^5 \cdot \rho} \propto \left\{ \frac{1}{R_{imp} - R_s} \int_{R_s}^{R_{imp}} [U_p(R) - U_f(R)]\, dR \right\}^2 \quad (10)$$

in which Eu is the mixing power number. In Equation (10), the proportionality symbol was used because the exact value of C_d and theoretical functional dependence of the mixing power P on the number of blades z is unknown (Furukawa et al., 2012; Nagata, 1975).

To determine the power by means of the method described, it is necessary to know the exact velocity distributions of the liquid inside the impeller. Limited data in the literature (Nagata, 1975) indicate a strong dependence of the mixing power on the location of the starting point of the velocity differences R_s. In order to obtain the relationship $Eu = f(R_s)$ for the 6FBT impeller working in a mixing tank without baffles, an exemplary numerical simulation was carried out as presented in Figure 2. The R_c value calculated from Equation (3) for the conditions included in the legend of Figure 2 is 30 mm, and the experimentally determined value of the power number is $Eu = 1.3$ (Furukawa et al., 2012; Nagata, 1975). Figure 2 also shows the simulation of the relationship $Eu = f(k)$ based on Equation (6). These simulations were carried out with Mathcad.

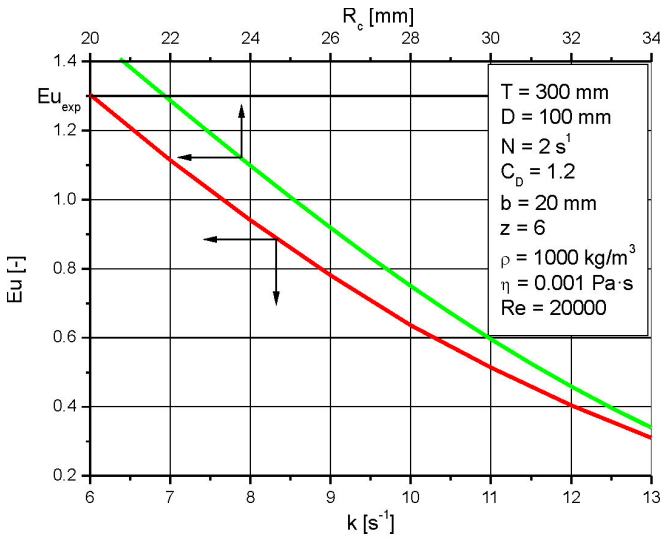

Figure 2. Exemplary dependence of the power number on the values of parameters R_c and k.

The simulation results confirm that it is not possible to agree R_c and k values at the same time so that the theoretical Eu value is equal to the experimental one. A separate problem was how to take into account in the calculations the number of impeller blades z. According to the principle applied in fluid mechanics, it was assumed that the total resistance of all impeller blades is the sum of the same resistance of many individual blades. The data in the literature (Beshay, 2001; Gzowska, 2019) indicate that in a tank with baffles, doubling the number of blades from 3 to 6 does not result in a twofold increase of the power number, but it increases only 1.6 times. Without baffles, this effect is even smaller, as the power increase factor is then 1.16 (Furukawa et al., 2012). This means that there are interactions between the blades and thus the results obtained for one blade cannot be easily extrapolated to a larger number of blades.

On the basis of the information presented, it can be expected that determining the mixing power based on the velocity distributions is a difficult task, especially in a mixing tank with baffles. Additionally, for a tank with baffles, the literature on the mixing process (Nagata, 1975; Paul et al., 2004; Stręk, 1981; Uhl and Gray, 1966; Zlokarnik, 2001) has not very much information about tangential velocity distributions. Since determining the velocity inside the impeller zone requires non-invasive measurement methods (such as LDA and PIV), the focus was on testing the velocity of the liquid leaving the impeller rotor. However, even these data for FBT mixers are insufficient. Much more information relates to the Rushton turbine, which is more often used in industrial practice (Ditl et al., 2018; Huchet et al., 2009; Lee and Yianneskis, 1998; Sharp and Adrian, 2001; Ståhl Wernersson and Trägårdh, 1998; Ståhl Wernersson and Trägårdh, 2000; Wu et al., 1989). This may change owing to the rapidly developing CFD techniques in recent years (Delafosse et al., 2009; Ducci and Yianneskis, 2006; Hargreaves et al., 2014; Joshi et al., 2011; Li et al., 2011; Sheng et al., 2000; Zadghaffari et al., 2010).

The goal of this study was first of all to determine the liquid flow maps and hydrodynamic changes that take place during emptying a tank with baffles with the operating 6FBT impeller. The second goal was to determine the tangential velocity profiles in the area of the impeller and to check the usefulness of Equation (10) for the determination of the mixing power. This is now facilitated by the development of non-invasive velocity measurement techniques (including Laser Doppler Anemometry – LDA, and Particle Image Velocimetry – PIV).

2. MATERIALS AND METHODS

2.1. Measurements of mixing power

Measurements of the mixing power while emptying the mixing tank were made in a flat-bottomed tank with a diameter of $T = 292$ mm equipped with four standard baffles ($B = 0.1 \cdot T$) and filled with water to a height of $H_0 = 300$ mm. The diameter of the 6FBT impeller was

$D = 100$ mm ($D \approx T/3$) and the center of its height was at a level of $H_m = D = 100$ mm above the tank bottom. For a blade height of $b = 20$ mm ($b = D/5$) this gives a clearance of $C = 90$ mm. The measurements were carried out in water ($t = 20$ °C) for four rotational frequencies of the impeller $N = 1.5$ s^{-1}, $N = 2.0$ s^{-1}, $N = 2.5$ s^{-1} and $N = 3.0$ s^{-1}. For these rotational frequencies, the Reynolds number for the mixing process was included within a range of $\mathrm{Re} = N \cdot D^2 \cdot \rho/\eta = 15000 \div 30000$ (for $\rho = 1000$ kg/m^3 and $\eta = 0.001$ Pa·s) and the Froude number within a range of $\mathrm{Fr} = 0.023 \div 0.092$. During the measurement, water was pumped out of the tank with a VERDER-FLEX 2010 peristaltic pump with a volumetric flow rate of $V_w = 1.356 \cdot 10^{-5}$ m^3/s, which resulted in the lowering of the liquid surface at a speed of $U_H = 0.202$ mm/s.

The mixing power was calculated on the basis of the torque measurements with an IKA EURO-ST P CV meter connected to a computer recording the instantaneous values of the rotational frequency N and the torque M with the sampling time $\Delta\tau = 2$ s. Then the mixing power P and power number Eu were calculated from classical equations.

2.2. PIV measurements

The tests were carried out in a mixing tank with a diameter of $T = 292$ mm in a geometrical configuration described in Section 2.1. Due to the curvature of the mixer walls, it was also placed in a rectangular tank filled with distilled water. Glass hollow spheres with an average diameter of 10 µm added to water were used as tracers. A PIV system (Raffel et al., 2007) by LaVision with a two-pulse Nd:YAG laser with a maximum power of 135 mW and an ImagePro camera with a resolution of 2048 px × 2048 px was used for velocity measurements.

Measurements of radial and axial velocities were made through the side wall of the tank at the stand: a diagram of this is shown in Figure 3a. The vertical plane of the light knife was symmetrical between the baffles or about 2° ahead of the baffle. The optical axis of the camera was perpendicular to the plane of the light knife. The use of a Vario-Pancolar 35–70 mm $f/2.7$–$f/3.5$ lens allowed a measurement field of approx. 280 mm×280 mm at the shortest focal length (this field did not include only the highest layer of water, approx. 20 mm thick). Measurements were made for the liquid height from $H = 300$ mm to $H = 110$ mm with the step $\Delta H = 10$ mm. The rotational frequency of the impeller was $N = 3$ s^{-1} ($\mathrm{Re} = 30000$, $\mathrm{Fr} = 0.092$). For each water height in the tank, a series of 300 double pictures of the flow markers in the tank was recorded with a frequency of 2.7 Hz (Heim and Stelmach, 2011) with a time interval of $\Delta\tau = 1900$ µs. After two-pass image processing in the DaVis 7.2 program, instantaneous velocity distributions were obtained in measurement fields with dimensions of 32 px × 32 px. Then the measurement data were averaged.

Measurements of tangential and radial velocities were made through the mixing tank bottom for five rotational frequencies of the impeller $N = 1.0$ s^{-1}, 1.5 s^{-1}, 2.0 s^{-1}, 2.5 s^{-1} and 3.0 s^{-1} and four liquid heights in the tank $H = 170$ mm, 180 mm, 190 mm and 200 mm. This corresponds to the range of Reynolds numbers from $\mathrm{Re} = 10000$ to $\mathrm{Re} = 30000$. In each case, the plane of the light knife was horizontal and was at a height of $H_m = 100$ mm above the tank bottom (Figure 3b). For each water height and rotational frequency, 300 double images were recorded with a frequency of 2.7 Hz ($\Delta\tau = 2600$, 1950, 1550, 1200 µs). Based on the data obtained, the distributions of the components of tangential and radial velocities in the mixing tank were determined (Stelmach, 2014).

3. RESULTS

3.1. Mixing power

Figure 4 shows the dependence of the mixing power on the relative height of the liquid in the tank $H^* = H/H_0$ while emptying the mixing tank, where H is the instantaneous

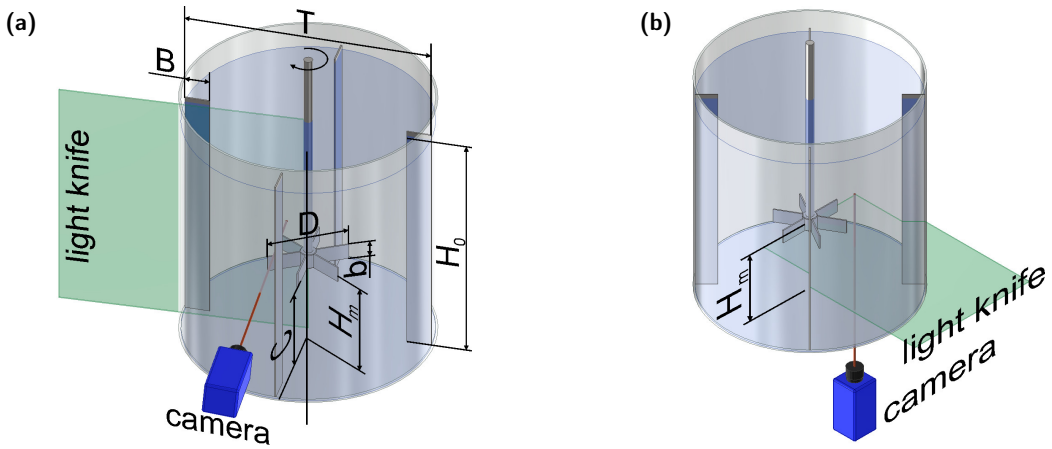

Figure 3. Diagram of the test stand with the PIV system for measuring radial and axial velocities (a) as well as tangential and radial velocities (b).

height of the liquid in the tank, and H_0 is the initial height of the liquid in the tank. When the impeller completely emerges from the liquid ($H = C$ and $H^* = 0.30$) it rotates in the air and the measured torque is close to 0.

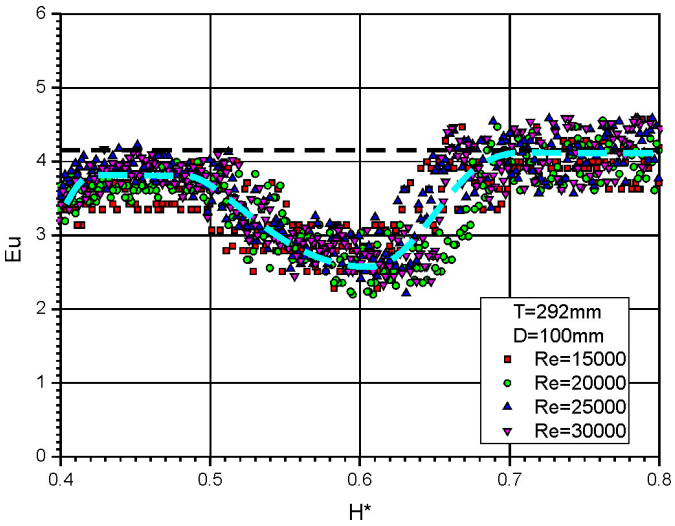

Figure 4. The dependence of the mixing power number on the dimensionless height of the liquid above the 6FBT impeller.

As can be seen in Figure 4 the courses of changes presented, $Eu = f(H^*)$, were repeatable and independent of the values of the Re number. Up to the value of $H^* \approx 0.65$, the mixing power number had a constant value of $Eu = 4.15 \div 4.20$. This value is close to the value reported in the literature, from $Eu = 4.0$ (Stręk, 1981) to $Eu = 4.4$ (Furukawa et al., 2012; Nagata, 1975; Paul et al., 2004). When the liquid level lowered further the power number value droppedsharply and on a smaller scale, it was slightly higher. After reaching the minimum power for $H^* \approx 0.60 \div 0.62$, it increased to a value close to that of a full tank. This Eu value remained in the range of H^* from 0.52 to 0.42 and then decreased to zero as the impeller slowly emerged from the liquid.

The significant decrease in the value of the power number Eu observed in Figure 4, which in the extreme case was even more than 40%, could not be accidental and must be related to the changes in the distribution of the liquid velocity in the mixing tank.

Using the measuring system shown in Figure 2a, the distributions of axial and radial velocities in the plane of the light knife in the r–z plane were obtained, and based on them the flow maps in the analyzed plane were determined. Figure 5a shows the circulation for the height of the liquid for a mixing tank completely filled with water, that is for $H^* = 1$ (due to measurement limitations, the image area did not include 20 mm of the water column from its free surface) in the radial-axial plane $R - H$ for which the dimensionless system $R^* = R/R_T$, $H^* = H/H_0$ was used. In order to generalize results, the dimensionless velocities $U^* = U/U_{tip}$ were used, where U_{tip} is the tangential velocity of the tip of the impeller blade $U_{tip} = \pi \cdot D \cdot N$. On the right side of each figure, there are also added values of the expression $(H-C)/T$ used in the works on changes of the mixing power during tank emptying.

The high layer of liquid above the impeller causes the liquid to flow axially between the blades. At the height of the impeller, the radial component of velocity is small. Only under the impeller does the flow direction change to radial. The radially flowing stream of liquid is slowed down at the wall and divided

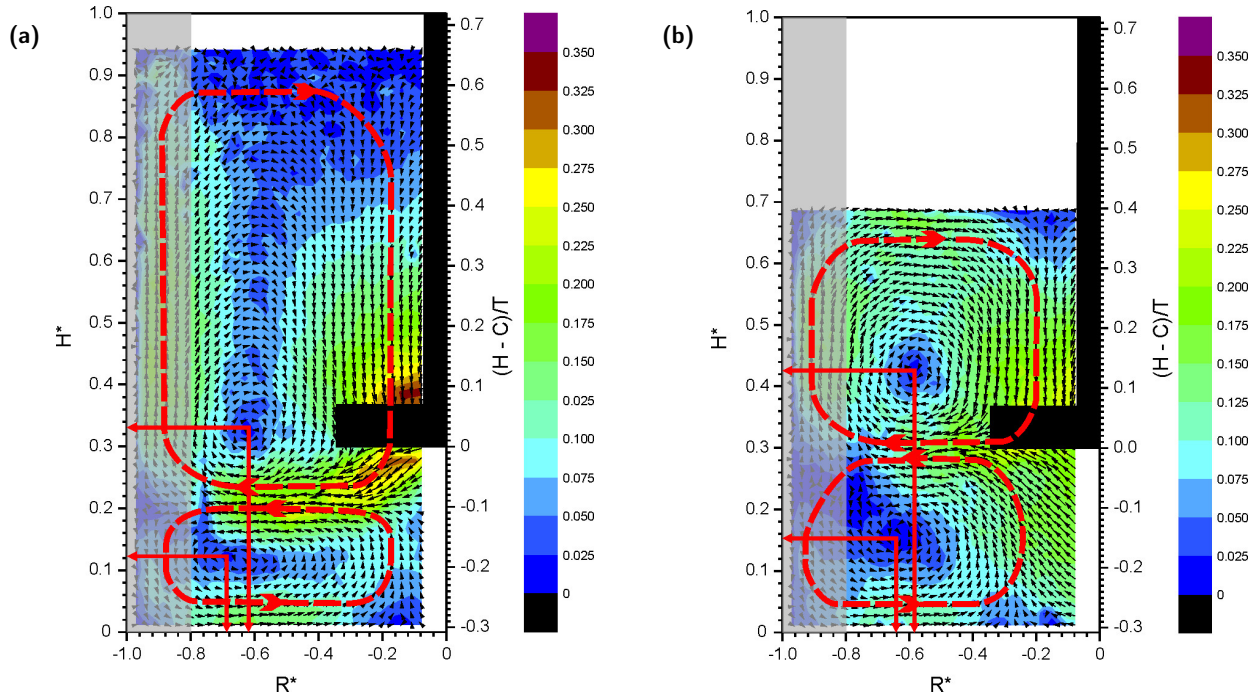

Figure 5. Flow patterns for $N = 3\ s^{-1}$ (Re = 30000, Fr = 0.092); (a) $H^* = 1.00$, (b) $H^* = 0.70$.

into two streams (circulation loops are marked in the figure with a red dashed line). Two circulation cores are observed of which the upper is located at the height of the impeller. For the liquid height discussed, a considerable drop in the velocity of the liquid outside the impeller is observed. The upper part of the mixing tank is very poorly mixed. Lowering the liquid level in the mixing tank to the value $H^* = 0.7$ reduces the axial flow (Figure 5b), while the radial flow increases. As a result, the upper circulation core moves above the impeller.

It should be noted that, although the two flows presented in Figure 5 differ in terms of different values of the resultant liquid velocities at corresponding points on both velocity maps, the nature of the flow is the same: in both cases in the mixing tank there are two secondary circulation vortices rotating in opposite directions. This means that the 6FBT impeller for $H^* > 0.7$ works all the time as a radial impeller in which the main liquid stream flows from the area of the impeller in the radial direction up to the value of $H^* \cong 0.63$ (Figure 6a) and, therefore, for this H^* range a line was obtained $Eu = 4.15 \div 4.20 = \text{const}$, as shown in Figure 4.

However, further reduction of the liquid level by only 10 mm – from $H^* = 0.63$ to $H^* = 0.60$ – caused a fundamental change in the circulation of the liquid in the mixing tank, which is shown in Figure 6b. Due to the constant reduction of the liquid space for the upper vortex, it disappears after some time, because there is no space for the upper vortex of radial-axial circulation (secondary circulation) to close above the impeller. The flow in the entire $R^* - H^*$ plane controls only one anti-clockwise vortex. The liquid flows vertically upwards through the impeller zone above it deviates radially towards the wall of the tank. This is a classic case of axial flow in a mixing tank, where the main liquid flow in the impeller zone is the vertical flow. As is known, axial flow is less energy-consuming than radial flow because the Euler power numbers for radial impellers are always several times higher than those for axial impellers (Nagata, 1975; Paul et al., 2004; Stręk, 1981). Therefore, in Figure 4 in the same range of changes of the H^* parameter, a fairly rapid reduction of the mixing power demand can be observed.

With further lowering of the liquid level, the way in which the liquid circulates inside the mixing tank is not changed formally because there is only one lower circulation vortex. However, the position of the circulation core is lowered (Figure 7), and for $H^* < 0.45$ the radial flow returns because the main stream flowing out of the impeller zone is again the radial stream. As a result, the value of the number Eu in Figure 4 takes the initial value.

On the basis of the analysis of power curves (Figure 4) and flows in the tank (Figures 5, 6 and 7), it can be concluded that rapid changes in the mixing power demand occur when the liquid circulation in the tank changes. The first change for $H^* \approx 0.65$ is when the radial-circumferential circulation changes to the axial-circumferential circulation and the second change for $H^* \approx 0.45$ is when the circulation change takes place in the opposite direction.

However, the qualitative description of the observed phenomenon presented does not allow conclusions to be drawn about the magnitude of the changes observed. As mentioned in the introduction, the observed energy changes must most

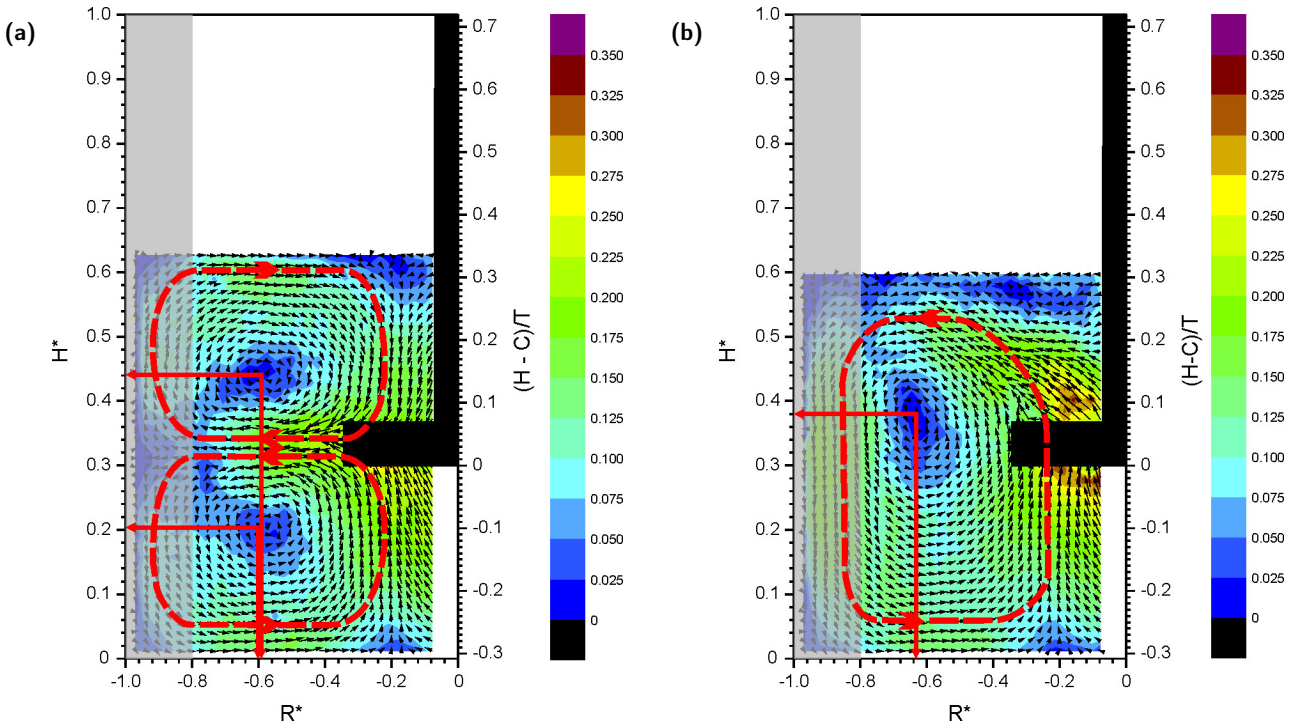

Figure 6. Flow patterns $N = 3\ \text{s}^{-1}$ (Re = 30000, Fr = 0.092); (a) $H^* = 0.63$, (b) $H^* = 0.60$.

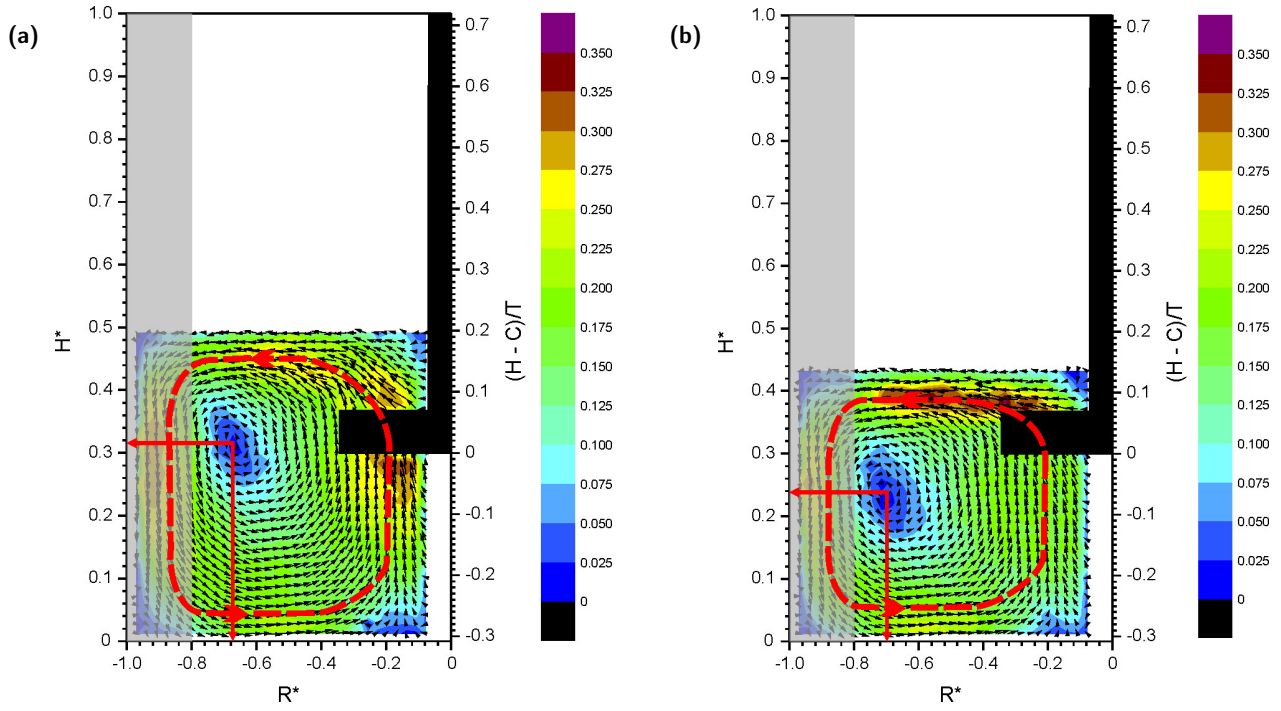

Figure 7. Flow patterns $N = 3\ \mathrm{s}^{-1}$ (Re = 30000, Fr = 0.092); (a) $H^* = 0.50$, (b) $H^* = 0.43$.

likely result from the changes in the values of the tangential velocities of the liquid in the impeller.

3.2. Velocity profiles, tangential and radial velocities

The velocity maps shown in Figures 5, 6, and 7 visualize the liquid flow in the mixing tank well, but the large amount of information contained in them makes detailed analysis difficult. Therefore, after the initial preparation of similar flow maps, but in the horizontal plane, as shown in Figure 3b, the velocity profiles obtained from these maps in the Origin 8.5 program were used to describe the hydrodynamic phenomena occurring in the impeller area.

Figure 8 presents the tangential velocity profiles obtained for a mixing tank without baffles at the impeller height $H_m = 100$ mm with the height of the free liquid surface in the mixing tank $H = 200$ mm. The black line in Fig. 8 means the dimensionless velocity $U_t^* = R^*/R_{\mathrm{imp}}^*$ of the impeller blade at the radius R^*. The profiles presented can be treated as reference ones to check the reliability of the measurement method obtained for the simplest case, that is a mixing tank without baffles. Due to the continuity of the liquid flow in the mixer, in Fig. 8 the relationship $U_t^* = f(R^*)$ was presented using line passing through the center of the measurement points but without points. The diagram shows the location of the radii R_{c1}^* and R_{c2}^* calculated from Equations (3) and (4) respectively. An analysis of Figure 8 shows that the maximum value of the tangential velocity is much closer to the tip of the impeller blade than that resulting from the central vortex theory and the value R_{c1}^* determined on its basis. However, the position of the maximum velocity is much better determined by the value R_{c2}^* calculated from Equation (4). The figure also shows the curve (dashed line) obtained from Equation (6) for $N = 2.5\ \mathrm{s}^{-1}$ and $k = 19.9\ \mathrm{s}^{-1}$ (the value of coefficient k was determined iteratively so as to obtain the best match to the experimental curve). This curve well represents the profiles of dimensionless tangential velocity outside the impeller area. However, there are noticeable differences inside the impeller, which at this stage of the research cannot be clearly commented on.

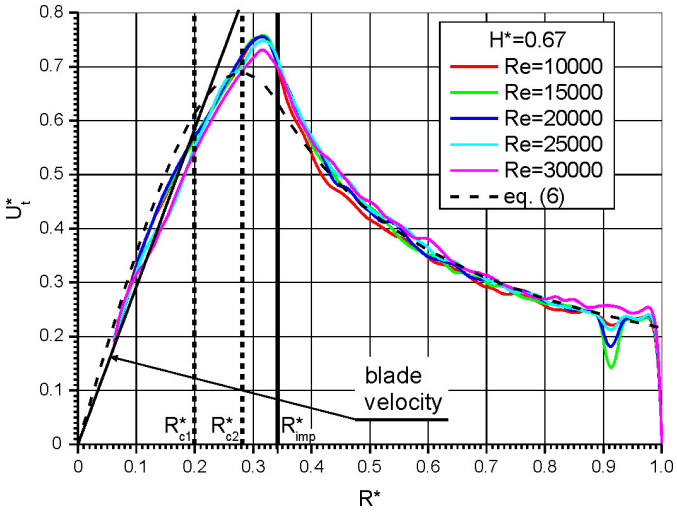

Figure 8. Profiles of dimensionless tangential velocities in the tank without baffles at the liquid height in the tank $H^* = 0.67$.

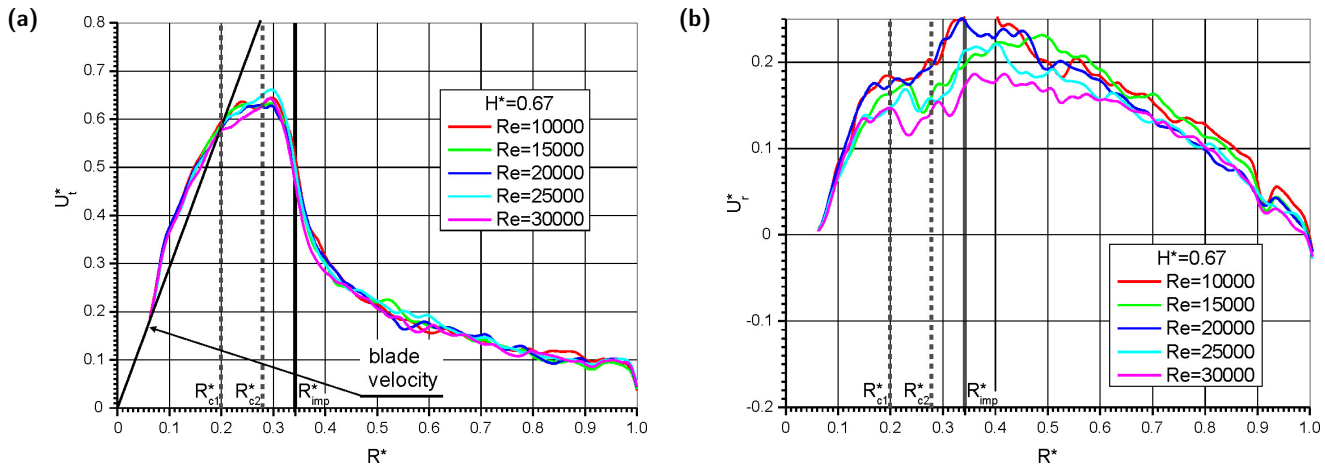

Figure 9. Profiles of dimensionless tangential (a) and radial (b) velocities for the height of the free surface of the liquid in the mixing tank with baffles $H^* = 0.67$.

Figure 9 shows the profiles of dimensionless tangential and radial velocities at the impeller height for the same height of the free surface of the liquid in the tank as in Figure 8 ($H =$ 200 mm), but with baffles. These profiles were determined for the line of intersection of the horizontal plane of the light knife with the vertical plane symmetrically placed between the baffles (this note also applies to Figure 10).

As can be seen in Figure 9, the circulation in the tank with baffles is still of a radial-tangential character, while positive values of the radial velocity indicate the flow towards the wall of the tank. The profiles of the dimensionless tangential component U_t^* for different rotational frequencies of the impeller practically coincide with each other. Starting from the radius R_{c1}^*, the tangential velocities of the liquid become lower than the blade velocity, as in the case of the mixing tank without baffles. However, further research is required to explain why for $R^* < R_{c1}^*$ tangential velocities of the liquid are higher than the blade velocity. The maximum value of velocity is achieved for $R^* \approx 0.3$ and is equal to $U_t^* \approx 0.64$. This value is significantly lower than the value $U_t^* \approx 0.76$ achieved without baffles. This means that the relative velocity of the blade and the liquid in this area is greater, which explains the greater mixing power for mixing tanks with baffles. For higher radius values, there is a rapid drop in velocity, which is faster than without baffles. In the case of the radial component, the liquid in the entire range of the radius of the mixing tank flows from the axis of the tank towards its wall, which is consistent with the velocity map in Figure 6a. This component reaches its maximum values for a radius slightly larger than that of the impeller radius R_{imp}^*. Further towards the wall, an almost linear decrease in the value of the radial velocity is observed. It should be noted that the dimensionless radial velocity is almost three times lower than the tangential velocity.

For the height of the liquid surface in the mixing tank $H^* =$ 0.60 ($H =$ 180 mm), there are changes in the shape of the curves (Figure 10).

Height $H^* = 0.60$ ($H =$ 180 mm) corresponds to the height of the liquid in the mixing tank when the radial circulation of the liquid in the impeller zone has already changed to the axial circulation (Figure 6b) and, therefore, large differences

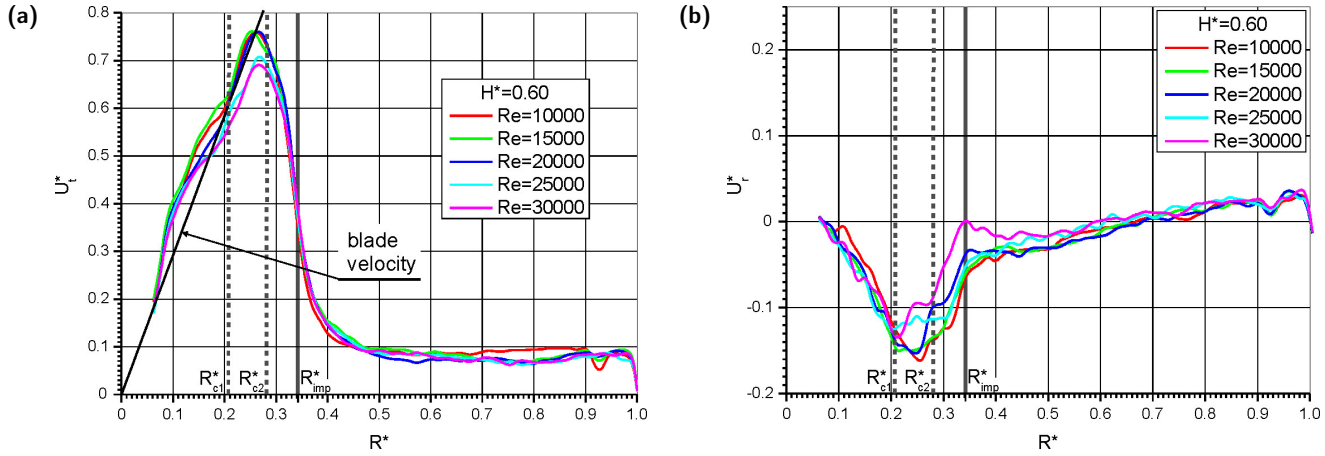

Figure 10. Profiles of dimensionless tangential (a) and radial (b) velocities for the height of the liquid $H^* = 0.60$.

in the distributions of both velocities are observed in Figure 9 and Figure 10. The differences between the tangential velocity of the liquid and the impeller blades are visible in this case only for $R^* \approx R^*_{c2}$ (Figure 10a) and practically for this point, the maximum liquid velocity is achieved $U^*_t \approx 0.75$ as in the absence of baffles. A small difference in tangential velocities and smaller active surface area of the tips of impeller blades result in a rapid decrease of mixing power (Euler number) observed in Figure 4. However, the decrease in velocity for larger radii is much faster than in the previous case shown in Figure 9a. For $R^* > 0.5$, the dimensionless tangential velocity stabilizes at a low level $U^*_t \approx 0.10$.

Greater changes in velocity distributions occur in the case of the radial component, where due to the reversal of the liquid circulation for $R^* < 0.6$, the flow direction is reversed and the liquid in the impeller zone flows towards the impeller axis, and the values U^*_r change the sign to the opposite, which can also be seen in Figure 6b. For the liquid height analyzed in the mixing tank $H^* = 0.60$, the difference between the velocities U^*_t and U^*_r is almost five-fold.

Further lowering of the liquid level in the mixing tank did not cause significant changes in the velocity profiles and the velocity distributions obtained correlated well with the flow maps presented in Figure 7.

The changes in velocity profiles discussed relate to the measurements in the vertical plane of the laser knife placed symmetrically between the baffles. The effect of the baffles on the circulation of liquid in other planes is undoubtedly significant and therefore in Figure 11 it was decided to compare the velocity profiles in the plane between the baffles and the one located next to the baffle (approx. 2° ahead of the baffle).

Outside the impeller up to $R^* \approx 0.4$, tangential velocity profiles in both cases are similar. However, at the baffle, due to its inhibitory effect, the tangential flow practically stops (Fig. 11b). For the same reason, the maximum dimensionless tangential velocities also decrease in the impeller plane from a value of 0.73 to a value of 0.65 (Figure 11). From the phenomenological point of view, it is completely understandable. Smaller maximum values of the circumferential component according to Equation (10) determine that in this measuring plane the amount of energy supplied by the impeller will be greater than in the area between the baffles.

The mechanism of changes in liquid circulation and motor loads presented in the study when emptying the tanks with an operating impeller for radial impellers (FBT) differs significantly from similar changes for the axial impellers (PBT) (Rieger et al., 2021; Stelmach et al., 2021a; Stelmach et al., 2021b). Figure 12 shows these differences schematically. For the FBT impellers, there are two periods of circulation change in the mixing tank: first from radial to axial circulation (left picture), then in the reverse direction. In the case of axial impellers (PBT), there is only one change from axial to radial circulation together with a related significant increase in power demand for the impeller drive (right figure). In both cases, after the impeller emerges from the liquid, the motor load drops to zero.

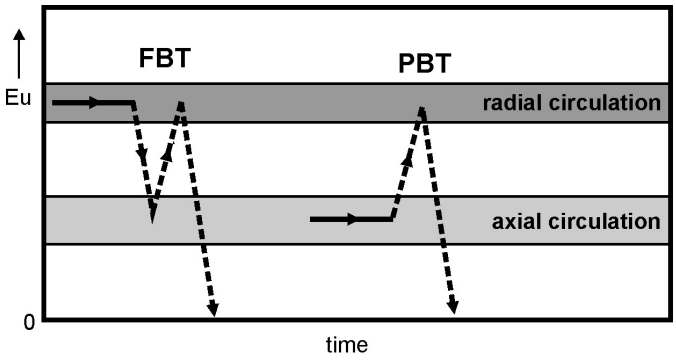

Figure 12. Effect of changes in the circulation in the mixing tank on the motor load.

In the case of radial mixers, changes in the liquid circulation in the mixing tank are of no practical importance for the selection of a drive motor, because the motor, in this case, is

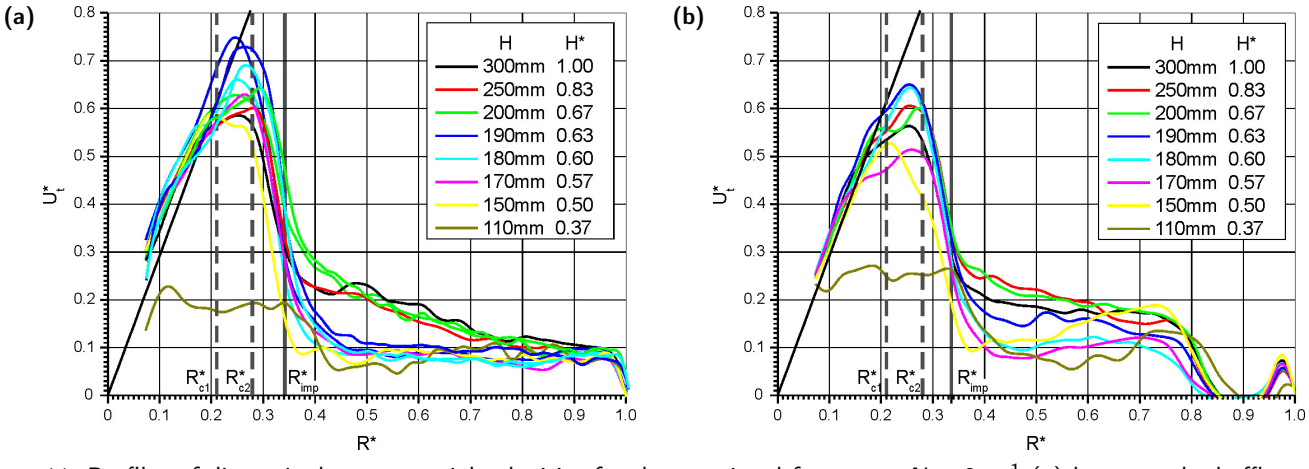

Figure 11. Profiles of dimensionless tangential velocities for the rotational frequency $N = 3\ s^{-1}$ (a) between the baffles, (b) at the baffle.

selected taking into account the large Euler numbers *Eu* for these impellers. Even if the motor is temporarily overloaded by 10–15%, the probability of motor damage is negligible. However, in the case of PBT impellers, where the motor is designed for low mixing power demand for axial impellers, even a few minutes of motor overload (in extreme cases even by 100%) may destroy it (Stelmach et al., 2021b).

As already mentioned, the velocity distributions specified in the study can be the basis for estimating the amount of energy expenditure needed to drive the 6FBT impellers for the variable height positions of the liquid surface in the mixing tank $H^* = H/H_0$.

3.3. Relationship between mixing power and relative velocity

Equation (10) shows that the energy transferred to the liquid by the blades is dependent on the relative velocity of the blade and the liquid. For the tangential velocity profiles obtained for different relative heights of the tank filling H^*, numerical integration can be performed to determine the integral mean of the difference in tangential velocities $\Delta\overline{U}$ of the impeller blade and the liquid inside the impeller zone along the blade radius and to calculate the value of the integral on the right side of Equation (10). Figure 13 shows the numerically calculated squares of the integral mean of velocity differences $[\sum(\Delta U_t^* \cdot \Delta R^*)]^2$ divided by the analogous value for the liquid height in the mixing tank $H^* = 1.0$. The value of this ratio should reflect the change in mixing power relative to the power requirement for a full tank.

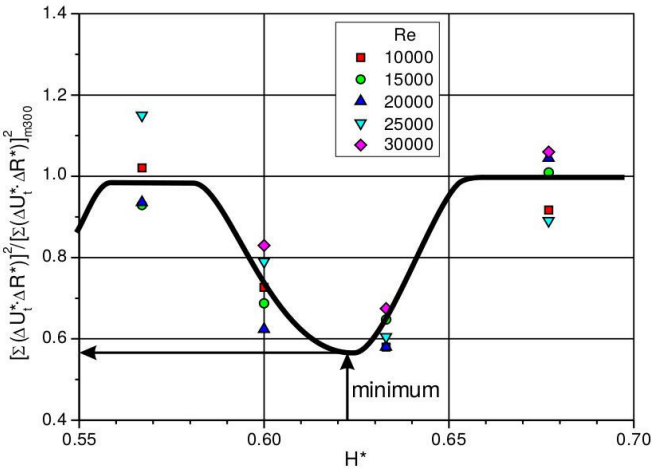

Figure 13. Relative mixing powers determined on the basis of the mean integral value of the difference of tangential velocities.

The curve obtained shows the mixing power minimum for the value $H^* = 0.63$, which represents well the course of the power curves presented in Figure 4. The qualitative compliance of the line course obtained and presented in Figure 4 and Figure 12 confirms to a great extent the proposed mechanism of changing the liquid circulation in the mixing tank when the level of the free surface decreases for radial mixers.

The proposed method of calculating the mixing power on the basis of the classical model of the central vortex or its modification is, however, not very precise because it is based on limited experimental data. Measurements were made only at one height and the instantaneous values in the space between the blades were averaged. To determine the drag force, a tangential velocity profile should be determined at a short distance ahead of the blade. This can be done with this method but requires the use of a trigger synchronized with the selected impeller blade.

4. CONCLUSIONS

In the case where the tank is emptied with an operating radial impeller (FBT impeller), a qualitative change of liquid circulation in the mixing tank takes place twice. At the relative height of the liquid level in the mixing tank $H^* \approx 0.65$, radial circulation of the liquid in the impeller zone changes to axial circulation, which results in a rapid decrease of the mixing power requirement, with a limit up to 40%. For $H^* \approx 0.45$ radial circulation returns. The reason for the changes is the lack of the required space above the impeller to close the secondary circulation line in the r–z plane.

The changes in the liquid circulation in the mixing tank are accompanied by the changes in the mixing power which for the FBT impellers run in the opposite direction than in the case of PBT impellers.

The proposed method of calculating the mixing power using the central vortex model and the integral mean of the difference between the tangential velocity of the blade and the liquid calculated by numerical methods is not very accurate. It can only be used to indicate relative power.

Increasing the accuracy of the above method will be possible with greater use of non-invasive research methods , such as PIV systems, taking into account the turbulence of the flowing liquid in the impeller zone or using CFD methods.

SYMBOLS

B	baffle width, m
C	clearance, m
D	impeller diameter, m
F	drag force, N
H	liquid height in the tank, m
H_m	distance of the impeller height center from the bottom, m
ΔH	step of the change of liquid height in PIV measurements PIV, m
M	torque, Nm
N	rotational frequency of the impeller, s^{-1}

R radius (generally), m
R_c central vortex radius, m
R_{c1} central vortex radius calculated from Equation (3)
R_{c2} central vortex radius calculated from Equation (4)
R_h hub radius, m
R_T radius of tank/mixing tank $R_T = T/2$, m
R_y vortex radius for the static liquid level determined with Equation (5), m
R^* dimensionless radius (generally), $R^* = R/R_T$
T tank diameter, m
U velocity (generally), m/s
U_r radial component of velocity, m/s
U_t tangential component of velocity, m/s
U^* dimensionless velocity $U^* = U/U_{\text{tip}}$, (generally)
U_H speed of lowering the liquid level, m/s
U_{tip} tangential velocity of the blade tip $U_{\text{tip}} = \pi \cdot D \cdot N$, m/s
U_f tangential velocity of the liquid, m
U_p tangential velocity of the impeller blade, m
V_w volumetric flow rate of water from the tank/mixing tank, m^3/s
z number of impeller blades, –
η dynamic viscosity, Pa·s
ρ density, kg/m^3
τ sampling time, s
ω angular velocity, s^{-1}

REFERENCES

Aiba S., Humphrey A.E., Millis N.F., 1973. *Biochemical engineering*. 2nd edition, University of Tokyo Press, Tokyo.

Beshay K., Kratěna J., Fořt I., Brůha O., 2001. Power input of high-speed rotary impellers. *Acta Polytech.*, 41, 18–23. DOI: 10.14311/280.

Campesi A., Cerri M.O, Hokka C.O., Badino A.C., 2009. Determination of the average shear rate in a stirred and aerated tank bioreactor. *Bioprocess Biosyst. Eng.*, 32, 241–248. DOI: 10.1007/s00449-008-0242-4.

Caşcaval D., Galaction A.-I., Turnea M., 2011. Comparative analysis of oxygen transfer rate distribution in stirred bioreactor for simulated and real fermentation broths. *J. Ind. Microbiol. Biotechnol.*, 38, 1449–1466. DOI: 10.1007/s10295-010-0930-3.

Delafosse A., Morchain J., Guiraud P., Liné, A., 2009. Trailing vortices generated by a Rushton turbine: Assessment of URANS and large eddy simulations. *Chem. Eng. Res. Des.*, 87, 401–411. DOI: 10.1016/j.cherd.2008.12.018.

Delvigne F., Destain J., Thonart P., 2006. A methodology for the design of scale-down bioreactors by the use of mixing and circulation stochastic models. *Biochem. Eng. J.*, 28, 256–268. DOI: 10.1016/j.bej.2005.11.009.

Ditl P., Šulc R., Pešava V., Jašíkova D., Kotek M., Kopecký V., Kysela B., 2018. Local turbulent energy dissipation rate in an agitated vessel, experimental and turbulence scaling. *Theor. Found. Chem. Eng.*, 52, 122–134. DOI: 10.1134/S0040579518010037.

Ducci A., Yianneskis M., 2006. Turbulence kinetic energy transport processes in the impeller stream of stirred vessels. *Chem. Eng. Sci.*, 61, 2780–2790. DOI: 10.1016/j.ces.2005.09.020.

Furukawa H., Kato Y., Inoue Y., Kato T., Tada Y., Hashimoto S., 2012. Correlation of power consumption for several kinds of mixing impellers. *Int. J. Chem. Eng.*, 2012, 106469. DOI: 10.1155/2012/106496.

Galaction A.-I., Cascaval D., Oniscu C., Turnea M., 2004. Enhancement of oxygen mass transfer in stirred bioreactors using oxygen-vectors. 1. Simulated fermentation broths. *Bioprocess Biosyst. Eng.*, 26, 231–238. DOI: 10.1007/s00449-004-0353-5.

Ghotli R.A., Raman A.A., Shaliza Ibrahim, Saeid Baroutian, 2013. Liquid-liquid mixing in stirred vessel: A reviev. *Chem. Eng. Commun.,* 200, 595–627. DOI: 10.1080/00986445.2012.717313.

Gzowska A., 2019. *Testing the mixing power and hydrodynamics of a new type of impeller for mixing biosuspensions*. MSc Thesis, Lodz University of Technology (in Polish).

Hargreaves D.M., Kakimpa B., Owen J.S., 2014. The computational fluid dynamics modelling of the autorotation of square, flat plates. *J. Fluids Struct.*, 46, 111–133. DOI: 10.1016/j.jfluidstructs.2013.12.006.

Heim A., Stelmach J., 2011. The comparison of velocities at the self-aspirating disk impeller level. *Przemysł Chemiczny*, 90/9, 1642–1646 (in Polish).

Huchet F., Liné A., Morchain J., 2009. Evaluation of local kinetic energy dissipation rate in the impeller stream of a Rushton turbine by time-resolved PIV. *Chem. Eng. Res. Des.*, 87, 369–376. DOI: 10.1016/j.cherd.2008.11.012.

Joshi J.B., Nere N.K., Rane C.V., Murthy B.N., Mathpati C.S., Patwardhan A.W., Ranade V.V., 2011. CFD simulation of stirred tanks: Comparison of turbulence models. Part I: Radial flow impellers. *Can. J. Chem. Eng.*, 89, 23–82. DOI: 10.1002/cjce.20446.

Lee K.C., Yianneskis M., 1998. Turbulence properties of the impeller stream of a Rushton turbine. *AIChE J.*, 44, 13–24. DOI: 10.1002/aic.690440104.

Li Z., Bao Y., Gao Z., 2011. PIV experiments and large eddy simulations of single-loop flow field Rushton turbine stirred tanks. *Chem. Eng. Sci.*, 66, 1219–1231. DOI: 10.1016/j.ces.2010.12.024.

Mazoch J., Rieger F., Jirout T., 2016. *Report TH 01020879, TECHMIX*, Brno, Czech Republic (in Czech).

Mohammed A.K., Hussen H.A., Al-Rassul S.A., 2008. Performance of gas induction in a dual – impeller agitated bioreactor. *Al-Khwarizmi Eng. J.*, 4(4), 1–8.

Nagata S., 1975. *Mixing: Principles and applications*. John Wiley & Sons, New York, NY, USA.

Ortiz X., Hemmatti A., Rival D., Wood D., 2012. Instantaneous forces and moments on inclined flat plates. *The Seventh International Colloquium on Bluff Body Aerodynamics and Applications* (BBAA7), Shanghai, China.

Ortiz X., Rival D., Wood D., 2015. Forces and moments on flat plates of small aspect ratio with application to PV wind loads and small wind turbine blades. *Energies*, 8, 2438–2453. DOI: 10.3390/en8042438.

Paul E.L., Atiemo-Obeng V.A., Kresta S.M., 2004. *Handbook of industrial mixing*. John Wiley & Sons: Hoboken, NJ, USA.

Raffel M., Willert C., Wereley S., Kompenhans J., 2007. *Particle image velocimetry. A practical guide*. 2nd edition, Springer Berlin, Heidelberg. DOI: 10.1007/978-3-540-72308-0.

Rieger F., Moravec J., Stelmach J., Kuncewicz Cz., 2021. Effect of modification of the stirrer with folding blades on the increase in mixing power during emptying the tank. *Przemysł Chemiczny*, 100/12, 1231–1235. DOI: 10.15199/62.2021.12.15.

Sharp K.V., Adrian R.J., 2001. PIV study of small-scale flow structure around a Rushton turbine. *AIChE J.*, 47, 766–778. DOI: 10.1002/aic.690470403.

Sheng J., Meng H., Fox R.O., 2000. A large eddy PIV method for turbulence dissipation rate estimation. *Chem. Eng. Sci.*, 55, 4423–4434. DOI: 10.1016/S0009-2509(00)00039-7.

Ståhl-Wernersson E., Trägårdh C., 1998. Scaling of turbulence characteristics in a turbine-agitated tank in relation to agitation rate. *Chem. Eng. J.*, 70, 37–45.

Ståhl-Wernersson E., Trägårdh C., 2000. Measurements and analysis of high-intensity turbulent characteristics in a turbine-agitated tank. *Exp. Fluids*, 28, 532–545. DOI: 10.1007/s003480050414.

Stelmach J., 2014. *Hydrodynamics of a two-phase liquid-gas system in a mixer – the use of photo-optical methods*. Lodz University of Technology (in Polish).

Stelmach J., Kuncewicz Cz., Adrian Ł., Jirout T., Rieger F., 2021b. Change in mixing power of a two-PBT impeller when emptying a tank. *Processes*, 9, 341. DOI: 10.3390/pr9020341.

Stelmach J., Kuncewicz Cz., Rieger F., Morawec J., Jirout T., 2020. Increrase of mixing power during emptying of tanks with turbine-blade impellers. *PrzemysłChemiczny*, 99/2, 239–243. DOI: 10.15199/62.2020.2.11.

Stelmach J., Kuncewicz Cz., Szufa S., Jirout T., Rieger F., 2021a. The influence of hydrodynamic changes in a system with a pitched blade turbine on mixing power. *Processes*, 9, 68. DOI: 10.3390/pr9010068.

Stręk F., 1971. *Mieszanie i mieszalniki*. WNT, Warszawa.

Stręk F., 1981. *Mieszanie i mieszalniki*. 2nd edition. WNT, Warszawa.

Uhl V.W., Gray J.B., 1966. *Mixing. Theory and practice*. Academic Press, New York & London, Vol. I, pp. 7–110.

Wu H., Patterson G.K., Van Doorn M., 1989. Distribution of turbulence energy dissipation rates in a Rushton turbine stirred mixer. *Exp. Fluids*, 8, 153–160. DOI: 10.1007/BF00195789.

Zadghaffari R., Moghaddas J.S., Revstedt J., 2010. Large-eddy simulation of turbulent flow in a stirred tank driven by a Rushton turbine. *Comput. Fluids*, 39, 1183–1190. DOI: 10.1016/j.compfluid.2010.03.001.

Zhao Y., Xiangyang Li, Jingcai Cheng, Chao Yang, Zai-Sha Mao, 2011. Experimental study on liquid–liquid macromixing in a stirred tank. *Ind. Eng. Chem. Res.*, 50, 10, 5952–5958. DOI: 10.1021/ie102270p.

Zlokarnik M., 2001. *Stirring. Theory and practice*. Wiley-VCH, Weinheim.